Investigation of Surface Enrichment in Isotopic Mixtures of Poly(methyl methacrylate)

I. Hopkinson, F. T. Kiff, and R. W. Richards*

Interdisciplinary Research Centre in Polymer Science and Technology, University of Durham, Durham DH1 3LE, U.K.

S. Affrossman, M. Hartshorne, and R. A. Pethrick

Department of Pure and Applied Chemistry, University of Strathclyde, Glasgow G1 1XL, U.K.

H. Munro

Courtaulds plc, Lockhurst Lane, Coventry CV6 5RS, U.K.

J. R. P. Webster

ISIS Science Division, Rutherford Appleton Laboratory, Chilton, Oxon OX11 0QX, U.K.

Received March 2, 1994; Revised Manuscript Received August 2, 1994®

ABSTRACT: The surface enrichment behavior of blends of perdeuterated poly(methyl methacrylate) with various molecular weights in a high molecular weight hydrogenous poly(methyl methacrylate) matrix has been studied using static secondary ion mass spectrometry and neutron reflectrometry. No significant enrichment was observed in any of these blends, and the results are interpreted in light of available diffusion and thermodynamic data. We conclude that the absence of surface enrichment is due to a low surface energy difference between hydrogenous poly(methyl methacrylate) and deuteropoly(methyl methacrylate) and believe this difference to be in the range 0.00–0.04 mJ m^{-2}. This is compared to the behavior of the hydrogenous polystyrene/deuteropolystyrene blends where the surface energy difference has been calculated to be 0.08 mJ m^{-2}.

Introduction

The surface composition of a polymer blend influences properties such as adhesion, solvent penetration, and wear resistance. Since the theoretical work of Cahn[1] in 1977, the field of "surface enrichment" in polymer blends has attracted continued theoretical and experimental interest.

There have been three main strands of theoretical work: phenomenological theories,[2–5] Monte Carlo models,[6,7] and models based on a Scheutjens–Fleer self-consistent mean-field lattice.[8–10] For binary blends where the components have the same degree of polymerization and the same segment volume ("symmetric" blends), these theories all indicate that the component of lower surface energy will enrich to the air surface and that the thickness of the enriched layer will be on the order of the radius of gyration of the enriching polymer. Enrichment at the surface leads to a variation of composition perpendicular to the sample surface. This variation can be expressed as a composition depth profile, $\phi(z)$, where $\phi(z)$ is the volume fraction of the enriching component at depth z. The precise shape of the composition depth profile, $\phi(z)$, is determined by the bulk properties of the blend: the interaction parameter χ and the molecular weights of the blend components. Low and negative values of χ indicate a more compatible blend and lead to thinner surface enriched layers. If we consider a blend, where the difference in surface energy between the components is kept constant, then as the χ decreases and becomes negative, the surface volume fraction predicted will decrease. The surface energy difference required to drive enrichment is very small. A difference of 2 mJ m^{-2} is enough to produce complete coverage of the surface with the low-energy component, and a difference of 0.05 mJ m^{-2} can lead to easily measurable enrichment.

The Scheutjens–Fleer type model of Hariharan *et al.* makes predictions for asymmetric blends, where the degrees of polymerization for the two components differ from each other. This model predicts that under certain circumstances entropic forces favoring lower molecular weight components can drive a low molecular weight component with higher surface energy to the surface.

A number of experimental techniques are available to test theories of surface enrichment. Techniques such as XPS and static SIMS can be used to determine composition just at the surface of a sample, with a probe depth of 10–50 Å. Ion beam techniques such as forward recoil elastic scattering (FRES),[11] dynamic SIMS,[12] and nuclear reaction analysis (NRA)[13] can provide composition depth profiles with a resolution ranging from 80 to 800 Å. Finally neutron reflectometry allows the near surface composition profile to be measured with a resolution of ~10 Å. Neutron reflectometry[14] is a scattering technique, and as such the data are a reciprocal space description of the density correlations in the sample. A direct transformation to real space is not generally possible, and consequently model fitting is used to obtain the composition depth profile from the data.

So far the deuteropolystyrene (d-PS)/hydrogenous polystyrene (h-PS) system has been the focus of the majority of work aimed at confirming the detailed predictions of surface enrichment theories. These blends are known to be immiscible,[15] particularly at high molecular weights; i.e., in certain composition and temperature ranges d-PS/h-PS blends will phase separate. It is found that the deuterated polymer has a

* To whom correspondence should be addressed.

® Abstract published in *Advance ACS Abstracts,* December 1, 1994.

0024-9297/95/2228-0627$09.00/0

slightly lower surface energy than the hydrogenous polymer due to the small difference in polarizability between the C−H and C−D bond. Jones *et al.*[16] have shown that the theory of Binder predicts the shape of the composition profile fairly well for symmetric high molcular weight blends. Hariharan *et al.*[17] have shown that their theory predicts the reversal of the isotope effect (i.e., d-PS depleting) which has been observed for low molecular weight h-PS blended with high molecular weight d-PS.

The aim of this work was to study the surface enrichment behavior of syndiotactic deuteropoly(methyl methacrylate) (d-PMMA)/hydrogenous poly(methyl methacrylate) (h-PMMA) mixtures. The kinetics of the enrichment were of particular interest. For comparison with the predictions of reptation theory,[18,19] we have studied thin films of a series of blends; in each case the same high molecular weight h-PMMA "matrix" was used with a constant volume fraction of probe d-PMMA. The molecular weight of the probe d-PMMA was varied between 12 000 and 420 000 for four different blends. These molecular weights span the entanglement molecular weight for PMMA of 30 000, and the blends were annealed over a wide range of "effective" annealing times, using the WLF equation to normalize annealing times over a range of temperatures to a single reference temperature. Static SIMS has been used to determine the composition at the immediate air/polymer interface, and neutron reflectometry has been applied in an effort to ascertain the form of the near surface composition profile.

Theory

Neutron Reflectometry. A neutron reflectometry experiment determines the variation of the intensity of a beam of neutrons reflected from a surface as a function of Q ($=(4\pi/\lambda)\sin\theta$, where θ is the angle of incidence on the surface of a neutron beam of wavelength λ), the scattering vector. The reflectivity, $R(Q)$, is defined as $I_r(Q)/I_0(Q)$, where $I_r(Q)$ is the reflected and $I_0(Q)$ is the incident intensity, λ is the neutron wavelength, and θ is the incident angle. The reflectivity $R(Q)$ provides information on the variation of scattering length density perpendicular to the sample surface,[20,21] $\varrho(z)$. The scattering length density of a polymer is given by:

$$\varrho = \frac{dN_A\sum b_i}{m} \tag{1}$$

where d is the physical density of the polymer, m is the repeat unit mass, N_A is Avogadro's number, and $\sum b_i$ is the sum of the scattering lengths of the atoms, i, in the monomer unit. The scattering lengths of ^{1}H and ^{2}H nuclei are very different and this means that composition gradients in polymer blends can be obtained from the scattering length density gradient if one component of the blend has been selectively deuterated. This is because scattering length density is additive, i.e., $\varrho(z) = \phi_D(z)\,\varrho_D + (1 - \phi_D(z))\varrho_H$, where ϱ_D and ϱ_H are the scattering length densities of the deuterated and the hydrogenous polymers, respectively, and $\phi_D(z)$ is the volume fraction of the deutero polymer as a function of depth. We will abbreviate $\phi_D(z)$ to $\phi(z)$.

Extracting the real space scattering length density depth profile, $\varrho(z)$, from the reflectivity data, $R(Q)$, is not straightforward. In general, there is no direct transform from $R(Q)$ to $\varrho(z)$; hence, a model fitting procedure must be used. The reflectivity of neutrons from a surface is entirely analogous to the reflectivity of electromagnetic radiation from a surface. The optical refractive index is simply replaced by the neutron refractive index, n:

$$n = 1 - \frac{\lambda^2}{2\pi}\varrho \tag{2}$$

This means that the reflectivity from a single uniform layer can be calculated using Fresnel's equations. The reflectivity of an arbitrary concentration profile can be calculated by representing the profile by a laminar structure where each sheet may have a different thickness and scattering length density. Using optical matrix methods, the reflectivity of this laminar structure can be calculated. The properties of the jth sheet in the structure are represented by the matrix:

$$M_j = \begin{pmatrix} e^{i\beta_{j-1}} & r_j e^{i\beta_{j-1}} \\ r_j e^{-i\beta_{j-1}} & e^{-i\beta_{j-1}} \end{pmatrix} \tag{3}$$

$$r_j = \frac{p_{j-1} - p_j}{p_{j-1} + p_j} \tag{4}$$

$$p_j = n_j \sin\theta_j = (n_j^2 - n_{j-1}^2\cos^2\theta_{j-1})^{1/2} \tag{5}$$

$$\beta_j = (2\pi/\lambda)n_j d_j \sin\theta \tag{6}$$

n_j and d_j are the neutron refractive index and the thickness of the jth layer, respectively. The reflectivity, R, is then given by:

$$R = \frac{M_{21}M_{21}^*}{M_{11}M_{11}^*} \tag{7}$$

M_{11} and M_{21} are elements of the resultant matrix, M_R, obtained as the product of all the individual matrices for each separate layer, i.e.

$$M_R = \prod_{j=1}^{n} M_j \tag{8}$$

This system of equations facilitates the extraction of the composition profile via a model fitting procedure. Standard nonlinear least-squares methods have been applied in the analysis of reflectivity data, but other methods are also available. These include maximum entropy,[26] simulated annealing,[22] and indirect Fourier transform[23] methods. The advantages of the other fitting methods are that they go some way to avoiding the problem of the fit settling at a local rather than a global minimum in the value of χ^2 (χ^2 is a measure of the goodness of fit) and they also do not have the problem of preselecting a functional form to describe the composition profile. There is still the problem that the reflectivity profile is not unique. Quite different composition profiles can have very similar reflectivity profiles, even without considering instrument resolution and the limited Q range available.

It is also possible to obtain some information more directly from the reflectivity profile by using the Born or kinematic approximation:

$$R(Q) = \frac{16\pi^2}{Q^4}|\varrho'(Q)|^2 \tag{9}$$

$\varrho'(Q)$ is the Fourier transform of the composition gradients ($\partial\varrho/\partial z$) in the sample. In the limit of large Q, $\varrho'(Q) \rightarrow \sum\delta(\varrho(z))$, where $\sum\delta(\varrho(z))$ is the sum of the "jumps"

Table 1. Properties of Polymers

polymer	M_w	M_w/M_n	T_g/°C	% syndiotactic
h-PMMA	994 000	1.3	124.4	76
d-PMMA	12 400	1.2	119.4	77
d-PMMA	25 200	1.1	103.5	76
d-PMMA	136 000	1.1	129.9	
d-PMMA	417 000	1.3	130.5	74

Table 2. Scattering Length Densities

	volume fraction of d-PMMA	scattering length density/Å^{-2} ($\times 10^6$)
silicon	N/A	2.095
h-PMMA	0	1.034
d-PMMA	1.0	6.792
blend A	0.174	2.036
blend B	0.171	2.019
blend C	0.178	2.059
blend D	0.174	2.036

in the scattering length density; i.e., at large Q, $\varrho'(Q)$ is directly related to abrupt changes in the scattering length density. Commonly such sharp changes in scattering length density are only observed at the air/polymer and polymer/substrate interface. Formally:

$$\lim_{Q\to\infty} R(Q)Q^4 = 16\pi^2 \sum(\delta(\varrho(z)))^2 \qquad (10)$$

This means that the air/polymer surface composition of a sample can be obtained directly from the value of the asymptote of $R(Q)$ Q^4 vs Q at large Q, if it can be arranged that the polymer and substrate have the same scattering length density. It should be noted that correct use of eq 10 presupposes that the background signal due to *scattering* from the sample and incoherent scattering have been properly subtracted.

Experimental Section

Materials. Hydrogenous poly(methyl methacrylate) (h-PMMA) and perdeuterated poly(methyl methacrylate) (d-PMMA) were prepared by anionic polymerization of the purified monomers in a tetrahydrofuran solution at 195K using 9-fluorenyllithium as initiator. After termination by addition of degassed methanol, the polymers were isolated by precipitation in hot hexane, filtered off, washed, and dried under vacuum at 313K for 1 week. Molecular weights were determined by size-exclusion chromatography using chloroform as the eluting solvent. Stereotacticity of the polymers was obtained using ^{13}C NMR,[24] and the glass transition temperatures (T_g) were obtained from differential scanning calorimetry. Details of the five polymers used here are given in Table 1.

Sample Preparation (Neutron Reflectrometry). Blends of each of the deuterated polymers with the high molecular weight h-PMMA were dissolved in a toluene solution. In each case the volume fraction of d-PMMA in the d-PMMA/h-PMMA mix was approximately 0.17. This composition was chosen so that the uniform blends would have the same scattering length density as the silicon substrate. These blends will be referred to as A (d-PMMA M_w = 12 400), B (d-PMMA M_w = 25 200), C (d-PMMA M_w = 135 600), and D (d-PMMA M_w = 416 800). The calculated scattering length densities of h-PMMA, d-PMMA, the silicon substrate, and the four blends are shown in Table 2. Thin films of each of these blends were spun cast onto 5-mm-thick polished silicon disks which had a diameter of 50 mm. No attempt was made to remove the native silicon oxide layer from the surface of the silicon. The thicknesses of the films obtained were measured using contact profilometry. The variation in thickness over the area of any one film was small, being less than 100 Å, and the film thicknesses were in the range 3000–4000 Å. Control of the thickness of the spun-cast films was obtained by varying the total polymer concentration of the casting solution.

Table 3. Annealing Program for the Neutron Reflectivity Samples

temp/°C	actual annealing time/min	effective annealing time/min	blend
138	1585	3.3×10^{-3}	A, D
145	140	0.1	B, C
145	270	1.9	A, D
145	1390	9.9	A, D
145	1430	10	A, B
150	60	60	A, D
150	100	100	A, B, C, D
150	500	500	A, D
150	800	800	A
150	1000	1000	A, B, C, D
150	3000	3000	A, D
155	64	5000	A, D
155	102	8000	A, D
155	191	15000	A
155	255	2000	D
155	640	5000	D
155	1420	1.1×10^5	B
160	270	1.0×10^6	A, B, C, D
165	80	1.0×10^7	C
165	1030	1.3×10^8	A, B, C, D
170	360	9.9×10^8	C
175	207	9.6×10^9	B, C, D
184	4230	1.7×10^{13}	A, B, C, D

Unannealed samples of each film blend were retained. In addition, films were annealed, under vacuum, over a wide range of effective annealing times. This was done by annealing the samples over a range of temperatures, T, and then converting the actual annealing times, t_{actual}, to effective annealing times, t_{ref}, at a single reference temperature, T_{ref}, using the WLF equation:[25]

$$t_{ref} = \frac{t_{actual}}{a_T} \qquad (11)$$

where

$$\log a_T = \frac{-C_1^0 (T - T_{ref})}{C_2^0 + (T - T_{ref})} \qquad (12)$$

T_{ref} was chosen to be 150 °C, and $C_1^0 = 32.2$ and $C_2^0 = 80.0$ (see ref 25).

The minimum annealing time, t_{actual}, used was ~1 h, and samples were annealed by placing them on large preheated metal blocks in the oven. Similarly, annealed samples were "quenched" by removal from the oven and placing them on large metal blocks at room temperature. This was to ensure that the heating and cooling times were small compared to the actual annealing times. Table 3 shows details of the annealing program.

Sample Preparation (SSIMS). The polymers used for the SSIMS analysis were the same as those used for neutron reflectometry. Two blends were prepared, corresponding to blend A and blend D used for the neutron reflectrometry; the volume fraction of d-PMMA used for both blends was 0.174. These blends were dissolved in a toluene solution and spun cast onto silicon wafers which had been cleaned with a sulfuric acid/peroxide mixture, i.e., retaining the native silicon oxide layer. The film thicknesses were approximately 5000 Å. Films were then annealed at 150 °C, under an argon atmosphere, for periods up to 15 days (2×10^4 min).

Reflectometry. All the reflectivity data used in this work were collected on a CRISP reflectometer using the ISIS pulsed neutron source at the Rutherford Appleton Laboratory, near Oxford, U.K.

The data were collected at two incident beam angles, 0.25° and 0.6°, and at both angles the wavelength range used was 2–6.4 Å. Neutrons were detected using a one-dimensional position-sensitive detector. The background due to scattering from the bulk sample was extrapolated from the intensity either side of the specular peak for each incident neutron wavelength in the incident beam, and this was subtracted from

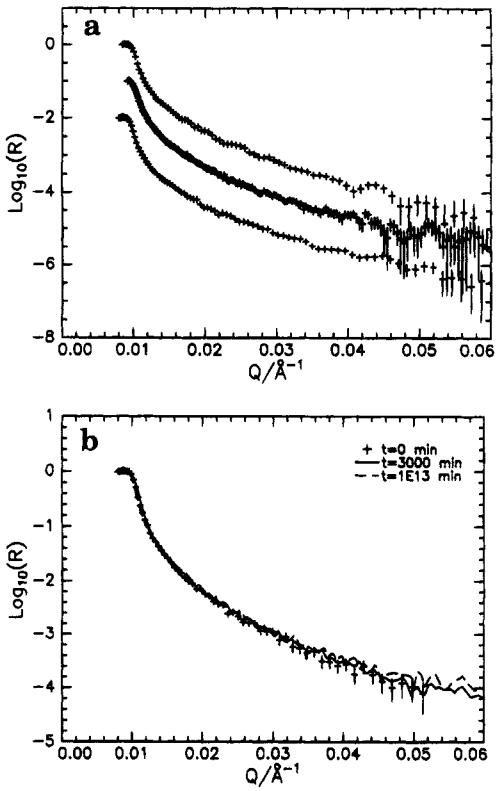

Figure 1. (a) Reflectivity profiles (log R vs Q) for blend C samples. Upper curve: unannealed sample, mid-curve sample annealed for 50 000 min (effective time). Lower curve: sample annealed for 1×10^{13} min (effective time). The latter two data sets have been offset by -1 and -2 units, respectively, for clarity. Error bars are those arising from Poisson counting statistics; the number of data points has been reduced for clarity. (b) Reflectivity profiles (log R vs Q) from blend D samples. Unannealed sample and samples annealed for 3000 min (effective time) and 1×10^{13} min (effective time). Overlaid to show a high degree of similarity between data.

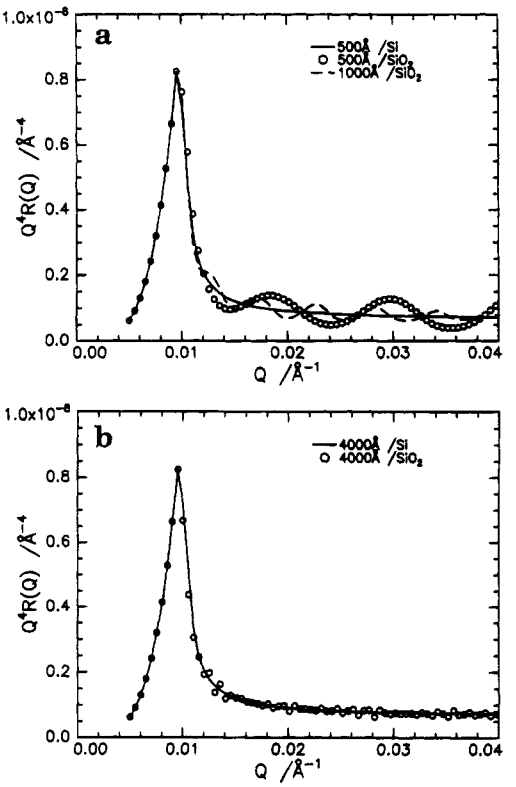

Figure 2. Calculated reflectivities (as RQ^4 vs Q plots) for thin films of d-PMMA/h-PMMA with a volume fraction of d-PMMA of 0.18. (a) (—) 500 Å layer on silicon; (○) 500 Å layer with 15 Å SiO_2 layer between silicon and polymer film; (- - -) 1000 Å layer with an intervening silicon oxide layer. (b) (—) 4000 Å layer on silicon; (○) 4000 Å layer with an intervening silicon oxide layer.

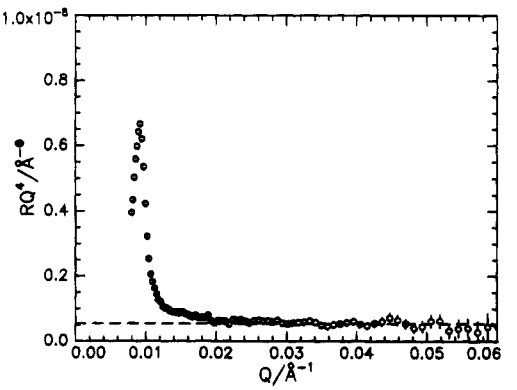

Figure 3. RQ^4 vs Q plot for blend C sample annealed for 1×10^{13} min (effective time). The broken line shows the value of the asymptote used to calculate the surface volume fraction of d-PMMA. Error bars show error arising from Poisson statistics.

the specular intensity. Detector efficiency corrections were made before any further analysis. The two sets of data overlapped in Q sufficiently such that they could be combined with no ambiguity, and the region of total reflection ($(R(Q) = 1)$, observed at low Q, was used to normalize the data to an absolute scale. All subsequent data analysis was carried out on these combined datasets which cover a Q range of 0.008–0.065 $Å^{-1}$. The resolution, in Q, arising from the geometry of the experiment was around 7%.

Static Secondary Ion Mass Spectrometry (SSIMS). SSIMS spectra were obtained using a Vacuum Generators 12–12 quadrupole mass analyzer. Vacuum Science Workshop mass-filtered ion and electron flood guns provided the incident beam and charge compensation, respectively. The incident beam of argon ions, at 3 keV and with a current measured at the ion gun of 0.2 nA, was focused onto *ca.* 5 mm^2 of the sample. The flood gun energy was set to 30 eV.

Results

Neutron Reflectometry. A representative selection of the reflectivity profiles obtained are shown in Figure 1. For clarity only the data from the unannealed samples are shown as points with error bars, and the number of points has also been reduced. The errors are calculated from Poisson counting statistics. The reflectivity profiles were all very similar. They were all smooth, had very similar critical edges, and differed only slightly at higher Q.

Before we describe the analysis procedures we have used for the reflectometry data, we address the possible artefacts that may be introduced by the retention of the native oxide layer on the silicon substrate. Since we have used a d-PMMA/h-PMMA composition which matches the scattering length density of silicon, the presence of this layer could be troublesome and have serious consequences for our data interpretation. To ascertain the possible effects, we have calculated the reflectivity (using optical matrix methods) for different thicknesses of this mixed PMMA layer on silicon and on silicon with a 15 Å layer of SiO_2 intervening. Each interface is assumed to be perfectly smooth for the purposes of the calculation. The results of these calculations are shown in Figure 2. For thin polymer films, i.e., less than 2000 Å thick, the influence of the oxide layer is clearly evident in the occurrence of fringes in the $Q^4R(Q)$ vs Q plot. However, for polymer film thicknesses of 3000–4000 Å as used by us, no influence

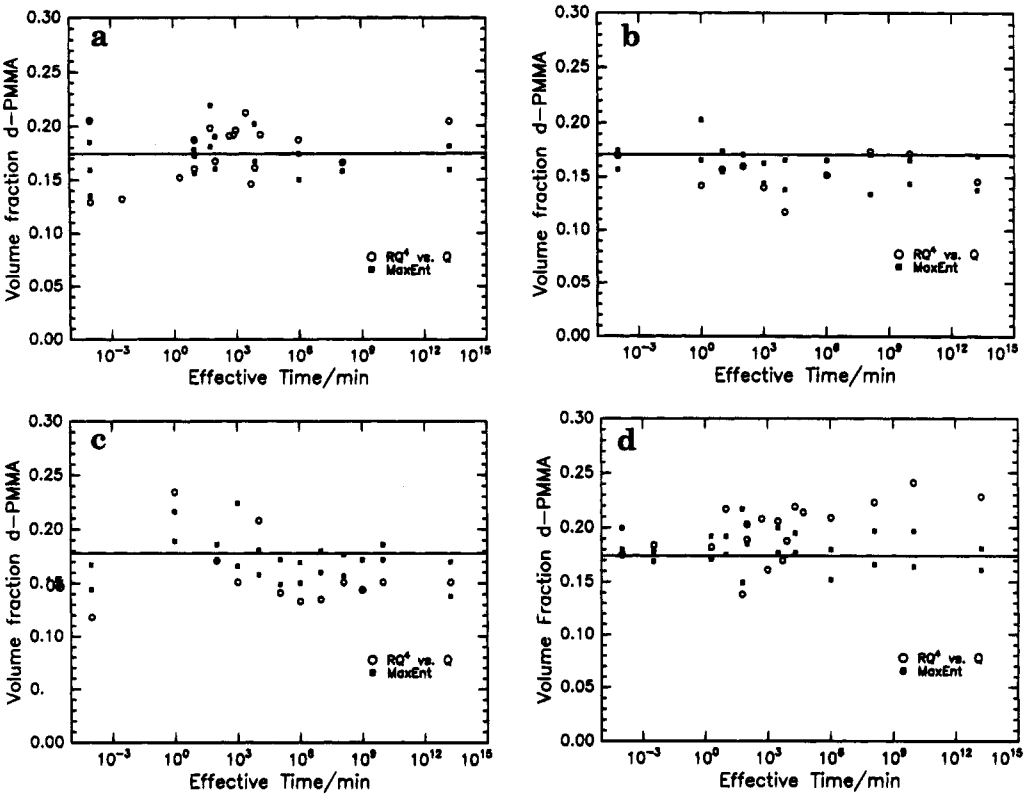

Figure 4. Air surface volume fractions of d-PMMA for (a) blend A, (b) blend B, (c) blend C, and (d) blend D. Open circles are data from RQ^4 vs Q asymptotes. Closed squares are from maximum entropy fitted profiles and indicate the range of volume fractions of d-PMMA found in the top 250 Å of the profile. Data from unannealed samples are placed at log(effective time/min) = −4. Data for two different unannealed samples are shown for blend A. Lines on each plot indicate nominal value of the bulk composition of the polymer mixture.

of this oxide layer is observed and consequently its presence does not have to be specifically accounted for in the analysis procedures detailed below.

The reflectivity data were analyzed in two ways: first, the values for the air/polymer interface volume fraction of d-PMMA were calculated from the asymptote at high Q of the RQ^4 vs Q plot; this was done for all the data collected. Figure 3 shows a typical RQ^4 vs Q plot. The asymptote was calculated over the Q range 0.03−0.048 $Å^{-1}$, and for this range the data appear to have reached a constant value. The data in the region 0.048−0.06 $Å^{-1}$ were excluded due to the observed larger statistical error. Statistical error in the surface volume fraction calculated from such asymptote values was in the range of 0.01−0.03. To evaluate the influence that surface roughness and the silicon/polymer interface have on the values of surface volume fraction calculated in this way, we calculated apparent surface volume fractions using this asymptote method from simulated data calculated using optical matrix methods. These calculations showed that, assuming a uniform layer, the silicon/polymer interface has no influence on the asymptote measured value of the surface volume fraction for the systems used here, although a systematic overestimation of the surface volume fraction was observed. The magnitude in volume fraction of the overestimation was 0.014. This error probably arises from the Q range used to calculate the asymptote being slightly too low; i.e., the RQ^4 vs Q plot has not reached its true asymptotic value, but increasing the Q range to higher Q leads to a larger statistical error. The effect of surface roughness is rather larger. Increasing the surface roughness at the air/polymer interface from 0 to 10 Å caused the surface volume fraction obtained from an RQ^4 vs Q plot to fall below that used to simulate the data, 0.158 being obtained when $\phi = 0.17$ was used. We have measured the surface roughness of spun-cast PMMA films using X-ray reflectivity and found that the air surface root-mean square roughness is around 5 Å. The combined effect of the silicon/polymer interface, surface roughness effects, and the slight overestimation due to the Q range used on the measured value of the surface volume fraction obtained from RQ^4 vs Q plots is likely to be a slight (<0.01) overestimation of the surface volume fraction. Figure 4 shows the values of the surface volume fraction calculated from using the asymptote method. Values for the unannealed films are shown at effective time = 10^{-4} min. Clearly for blends A−C no enrichment of d-PMMA to the air surface is observed. It would seem possible that a very small amount of surface enrichment is observed in blend D, using the asymptotic method of calculating the surface volume fraction of the d-PMMA, but the "enriched" surface volume fraction observed is only slightly outside the error range derived from the sources we have discussed.

Second, a large subset of the data were analyzed via optical matrix methods utilizing a maximum entropy procedure[26] to fit a free form model of 150 layers of fixed thickness. Figure 5 shows examples of composition profiles obtained in this way, with the data sets offset by a factor of 0.1 for clarity. Figure 4 show the values of the minimum and maximum volume fractions of d-PMMA found in the top 250 Å, obtained from these free form fits. The uncertainty in the minimum and maximum volume fractions of d-PMMA in the top 250 Å, arising purely from the Poisson counting statistics of the data, is in the range 0.005−0.01. These maximum entropy fits appear to show weak concentration gradients in all the films, even the unannealed films. The variation in the volume fraction profile between the unannealed films is as large as the variation between an unannealed film and an annealed film. There are

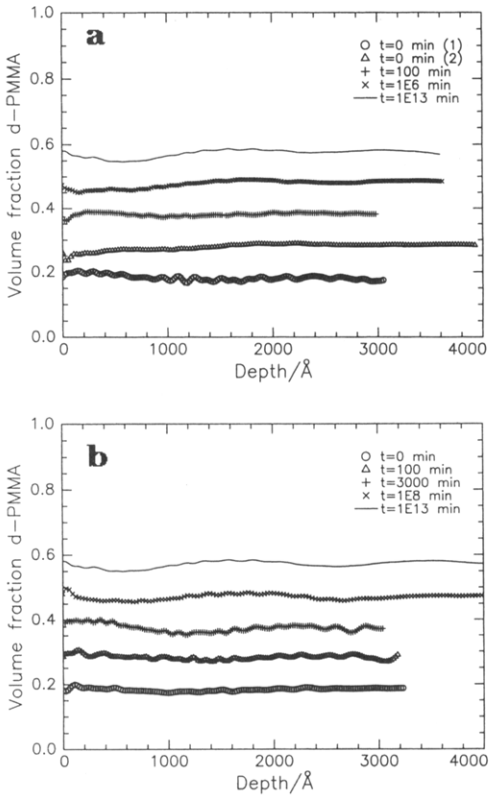

Figure 5. Selected volume fraction vs depth profiles, obtained using maximum entropy methods: (a) blend A and (b) blend D. Profiles are offset by 0.1 for clarity.

two explanations for this behavior: either these composition gradients really exist in the films and they arise during the spin-casting process or they are an artefact of the data analysis. If the gradients arose from the spin casting, it would be expected that during annealing the gradients in the bulk of the sample would be removed. Free energy is required to maintain concentration gradients and so the free energy of the system is reduced by removing the bulk concentration gradients. Several of the composition profiles show very similar variations in composition through the bulk of the specimen, characterized by a small-amplitude, low-frequency spatial variation in volume fraction. A similar pattern appears in different blends and for different annealing times which would suggest that it is an analysis artefact rather than actual structure. Such a low spatial frequency artefact could arise from a small systematic misfitting near the region of total reflection. The cause of this misfitting could be either use of an incorrect experimental resolution or absorption effects which were not incorporated in the fitting procedure. Inclusion of these latter effects has no significant influence on the values of the volume fraction, and therefore we conclude that the free form model fits indicate that no surface enrichment occurs in any of these blends, in complete agreement with results obtained by the asymptotic analysis. Although not reported here, we have also attempted to analyze the reflectivity data using an exponential functional form fit as suggested by the mean-field theory of Schmidt and Binder referred to above. The fits to the reflectivity data were rather unsatisfactory and produced air surface volume fractions which varied about an average value indicative of no surface enrichment in a manner similar to the two analysis procedures described above. Although the maximum entropy method is computationally more demanding, it has the benefit that no assumptions are made about the shape of the surface enrichment profile (if one exists).

Given the possible resolution problems, it may still be possible that any surface enrichment is confined to a length scale smaller than the resolution of the reflectometer. For this reason blends A and D were investigated by SSIMS.

SSIMS. The surface compositions of the unannealed and annealed blends were determined from the ratios of the peak intensities, I_m, of corresponding hydrogenous and deuterated fragments (with mass m) in the SSIMS spectra, assuming that the SSIMS sensitivities are not affected by isotopic substitution. Previous work on poly(styrene-d_8–styrene) showed no evidence of isotope effects on the relative SSIMS yields of corresponding light and heavy fragments.[27] The SSIMS fragmentation patterns for h-PMMA and d-PMMA have been reported by Brinkhuis and Ooij.[28] Two sets of hydrogenous and deuterated fragments were chosen for calculation of the compositions

1. CH_3^+ (relative molecular mass (rmm) = 15) and CD_3^+ (rmm = 18)

2. $C_4H_5O^+$ (rmm = 69) and $C_4D_5O^+$ (rmm = 74)

corresponding respectively to the ester methyl group (1) and a backbone fragment $H_2C{=}C(CH_3){\cdot}CO^+$ (2).

Most annealed films were found to be contamined by the well-known siloxane surface impurity, with a characteristic signal at rmm = 73, $(^{12}CH_3)_3Si^+$. This fragment has an associated species, $(^{13}CH_3)(^{12}CH_3)_2Si^+$, at rmm = 74 due to the natural abundance of ^{13}C, which contributes to the measured $C_4D_5O^+$ intensity. Such contaminants are difficult to remove, and cleaning procedures could lead to a change in surface composition. Hence, the intensity of the $C_4D_5O^+$ peak at rmm = 74 was corrected for $Si(^{13}CH_3)(^{12}CH_3)_2^+$ contamination by subtracting the intensity of the related $Si(^{12}CH_3)_3^+$ at rmm = 73 multiplied by 3 times the natural abundance of ^{13}C, i.e.

$$I_{74}(\text{corrected}) = I_{74}(\text{meas}) - I_{73}(\text{meas}) \times (3 \times \text{natural } ^{13}\text{C abundance})$$

The natural abundance of ^{13}C is 1.10%, and the factor of 3 arises from the fact that there are three carbons in the siloxane fragment. This correction was applied before any further analysis. All subsequent references to I_{74} refer to I_{74}(corrected).

Ideally the ratios $I_{18}/(I_{15} + I_{18})$ and $I_{74}/(I_{74} + I_{69})$ for the pure homopolymers should be 1.0 for d-PMMA and 0.0 for h-PMMA. Experimentally we found:

	$I_{18}/(I_{15} + I_{18})$	$I_{74}/(I_{74} + I_{69})$
h-PMMA	0	0.05
d-PMMA	1.0	0.92

The methyl signals (I_{18} and I_{15}) gave the expected values and could therefore be used directly to give the surface composition. The ratios calculated from the backbone fragments (I_{74} and I_{69}) differed slightly from the expected values. The probable cause for the discrepancy for pure d-PMMA was a small amount of hydrogenous contaminant. A rmm = 69 signal is frequently observed from common hydrogenous impurities, and this contribution would reduce the calculated ratio from the theoretical value. The nonzero ratio for the h-PMMA probably arises from an intrinsic rmm =

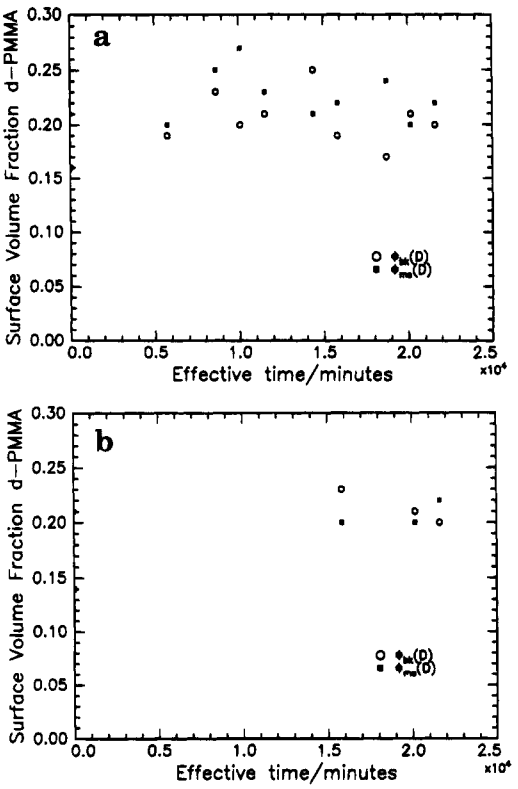

Figure 6. Surface volume fractions of d-PMMA obtained using SSIMS, for (a) blend A and (b) blend D. Values for the closed squares are calculated from the ester methyl fragment, and values for the open circles are calculated from the backbone fragment.

74 contribution. The monomer fractions of d-PMMA at the sample surface, calculated from the methyl ester $\phi_{me}(D)$ and the backbone fragment $\phi_{bk}(D)$ are given by:

$$\phi_{me}(D) = I_{18}/(I_{15} + I_{18}) \quad (13)$$

and, allowing for contaminants in the pure polymers,

$$\phi_{bk}(D) = [I_{74}/(I_{74} + I_{69}) - 0.05]/[0.92 - 0.05] \quad (14)$$

For these blends the monomer fraction is effectively identical to the volume fraction used in the analysis of the neutron reflectometry data.

Figure 6 shows values of the surface volume fraction of d-PMMA, obtained from the ester methyl fragments and the backbone fragments for blend A and blend D. The statistical error in any one value for the surface volume fraction is around 10%, arising purely from uncertainty in the measurement of peak intensities in the SSIMS experiment. The depth sampled with SSIMS is approximately 10 Å. Ignoring, for the momment, the unannealed values obtained from the $I_{74}/(I_{74} + I_{69})$ signals, the data indicate approximately constant surface compositions. The $I_{74}/(I_{74} + I_{69})$ values for the unannealed samples are, however, exceptions, being lower than the other data points in the set, including the $I_{18}/(I_{18} + I_{15})$ ratio. The most probable cause of the depression of the unannealed $I_{74}/(I_{74} + I_{69})$ values is a change in the contaminant level on heating the films. As noted above, the annealed films tended to acquire siloxane contamination. During heating, the original contaminant, with a signal at rmm = 69, may be reduced by desorption, diffusion into the bulk, or displacement by the siloxane contaminant. The net result is a decrease in the I_{69} signal after annealing. The $I_{18}/(I_{18} + I_{15})$ ratios would be little affected by the usual contaminants, and the unannealed and annealed values for these fragments are observed to be similar. For both blends these results show that the surface volume fraction of d-PMMA is unchanged by annealing but that the volume that it assumes appears to be slightly above the expected bulk value. The average value of the surface volume fraction for all the annealed blend A data is 0.21 ± 0.01, and the value for blend D is 0.22 ± 0.03. It is not clear whether this represents an enrichment of the d-PMMA to the air surface or whether it is the result of some systematic error that has not been accounted for.

Our conclusion from the SSIMS and the neutron reflectometry data is that no unambiguous signs of surface enrichment are observed in the d-PMMA/h-PMMA blends that we have studied.

Discussion

There are a number of possible explanations as to why no surface enrichment was observed in the d-PMMA/h-PMMA systems studied here:

(1) Insufficient annealing time was allowed for the surface enriched layer to form.

(2) The Flory–Huggins interaction parameter, χ, is too negative; i.e., the blends are too distant from the coexistence curve for enrichment to occur.

(3) There is insufficient surface energy difference between the d-PMMA and h-PMMA to drive surface enrichment.

The WLF equation has been used by other workers[21,29] to increase the effective annealing time domain. Use of the WLF equation (i.e., annealing at different temperatures) implies the belief that the polymer specimen under consideration is effectively ideal; i.e., there are no excess thermodynamic interactions. SANS measurements by us have shown that the interaction parameter, χ, for d-PMMA/h-PMMA mixtures varies with temperature such that phase behavior is expected, which is in common with other hydrogenous/deutero polymer blends such as polybutadiene[30,31] and polystyrene,[32] and we discuss this further when we consider item 2 above.

An alternative method of normalizing the annealing data is by consideration of the low molecular weight component diffusion coefficient, D^*. Recently Liu *et al.*[33] published such data for blends of a series of d-PMMA molecular weights in a matrix of h-PMMA (M_w = 980 000). These polymers were ~40–50% syndiotactic and as such had glass transition temperatures consistently lower than those of the polymers we used, which are 70–80% syndiotactic. Liu *et al.* find that:

$$D^* = kM_w^{-\alpha} \quad (15)$$

where $k = 1.8 \times 10^{-6}$ cm^2 s^{-1} g^{-1} mol

$$\alpha = 2.0$$

The data, from which this expression was derived, were collected at 145 °C. An Arrhenius type expression is used to describe the temperature dependence of the diffusion coefficient:

$$D^* = D^0 \exp(-Q/RT) \quad (16)$$

where Q is an activation energy. Van Alsten and Lustig[34] have measured this to be 109 kJ mol^{-1}. Combining these two expressions for the diffusion coefficient, we find:

$$D^* = k' M_w^{-\alpha} \exp(-Q/RT) \quad (17)$$

where $k' = 7.14 \times 10^6$ cm^2 s^{-1} g^{-1} mol.

This expression allows us to estimate the diffusion coefficient for a probe d-PMMA in a h-PMMA matrix with $M_w \approx 10^6 M_w$ over a range of temperatures and d-PMMA molecular weights. In an attempt to allow for the effect of the differing tacticities of the polymers used in Liu's work compared to ours, we will calculate diffusion coefficients using T_g as a reference. Table 4 shows variation of the diffusion coefficients, estimated using eq 17, over the range of temperatures used in the annealing program. The quantity of interest when determining how far toward equilibrium the system has been annealed is the diffusion length $(Dt)^{1/2}$, where t is the actual annealing time. These diffusion lengths are also included in Table 4. By this measure the range of effective annealing times used is far smaller than the range calculated by the WLF equation and shown in Table 3.

Jones and Kramer[35] have studied the kinetics of enrichment for the d-PS/h-PS system, and they derive several approximate expressions for the rate of growth of the surface excess z^*. In particular, the characteristic time, t_{eq}, for the approach to equilibrium is given by:

$$t_{eq} = \left(\frac{z_{eq}^*}{\phi_\infty}\right)^2 \frac{1}{D} \quad (18)$$

So the diffusion length for equilibrium to be achieved is of order $(Dt_{eq})^{1/2}$, and this can be calculated from the surface excess and the bulk volume fraction of d-PMMA. The phenomenological theory of surface enrichment predicts that the surface enrichment composition profile will be approximately exponential in form and that the decay length of the exponential will be on the order of the radius of gyration of the enriching polymer. The radii of gyration of the deutero polymers used in this work are approximately 30, 40, 95, and 165 Å for blends A–D, respectively. The surface volume fraction of d-PS observed in the d-PS/h-PS blends is around 0.6. Using these values we would expect to require a diffusion length on the order of 75 Å for blend A and 410 Å for blend D for surface equilibrium to be reached. The characteristic diffusion length for equilibrium is proportional to the surface excess, and so for smaller surface excesses we expect to find proportionally smaller equilibrium diffusion lengths. Comparing these estimates of equilibrium diffusion lengths with the range we believe we have accessed, then by these criteria some surface enrichment should be observable in all of the blends examined. We conclude that insufficient annealing is not responsible for the lack of observable surface enrichment.

The value of χ for a binary blend and the difference between the surface energies of the two components both affect the expected surface volume fraction. Recently we have measured[36] χ for two of the blends used in this work (B and D), using small-angle neutron scattering. These data give the following expressions for χ:

$$\chi = -0.12 + \frac{52}{T} \text{ (blend B)} \quad (19)$$

$$\chi = -0.003 + \frac{1.56}{T} \text{ (blend D)} \quad (20)$$

These data indicate that the higher molecular weight blends were annealed rather closer to the phase boundary than the lower molecular weight blends, given these values for χ and assuming that the surface energy difference between h-PMMA and d-PMMA is the same as that between d-PS and h-PS (i.e., 0.08 mJ m^{-2}), we would predict insignificant amounts of enrichment for the low molecular weight blends (A and B) but significant amounts of enrichment for the highest molecular weight blend (D and possibly blend C). Surface enrichment profiles for blend D, calculated using the expressions derived by Jones and Kramer are shown in Figure 7, which assumes that the two components of the blend have the same degree of polymerization. The χ parameters used in Figure 7a are the extremes of the range of values we calculate for our annealing program. This figure shows how the surface-enriched layer becomes much thicker as the coexistence curve is approached, i.e., as χ increases. The differences in surface tension, used in Figure 7b, range from the value found in the d-PS/h-PS system downward. For the systems modeled here the surface enrichment is virtually zero when the surface energy difference is 0.02 mJ m^{-2}. Entropic forces, favoring the low molecular weight species at the surface, will enhance the surface enrichment slightly, the effect being largest for blend A and smallest for blend D.

Table 4. Diffusion Coefficients and Diffusion Lengths

	diffusion coefficients/cm^2 s^{-1}			diffusion length range/Å	
blend	145 °C	160 °C	184 °C	low	high
A	4.7×10^{-15}	1.5×10^{-14}	7.8×10^{-14}	520	14100
B	1.1×10^{-15}	3.6×10^{-15}	1.9×10^{-14}	310	6940
C	3.9×10^{-17}	1.2×10^{-16}	6.5×10^{-16}	60	1290
D	4.1×10^{-18}	1.3×10^{-17}	6.9×10^{-17}	15	420

Surface enrichment can be driven by surface energy differences too small to measure directly. Experiments on the competitive adsorption[37] of d-PS and h-PS from solution onto SiO show an isotope effect, with the d-PS adsorbing preferentially. In contrast, similar experiments[38] using PMMA show no isotope effect. Granick attributes this difference to the fact that PMMA interacts with the SiO surface via the carbonyl bond, which is not subject to the effects of deuterium isotope substitution. We have attempted to calculate the surface energy of d-PMMA relative to that of h-PMMA using the parachor.[39] The parachor predicts surface energy by adding terms from the atomic composition and structural features such as double bonds and rings together. No data are available for the contribution of the deuterium atom. We estimated the deuterium contribution from the known difference in surface energy between h-PS and d-PS, and then used this deuterium term to calculate the surface energy of d-PMMA. We also calculated the surface energy for h-PMMA using the parachor. The difference between these calculated surface energies is 0.06 mJ m^{-2}, about 75% of the difference between d-PS and h-PS. Clearly this is a fairly crude calculation, but it does indicate that the expected surface energy difference between d-PMMA and h-PMMA is rather less than that between d-PS and h-PS. The SSIMS and neutron reflectivity data that we present here suggest that the surface energy difference between d-PMMA and h-PMMA is in the range 0.0–0.04 mJ m^{-2}.

Tasaki *et al.*[40] have published neutron reflectivity data that indicate enrichment of d-PMMA does occur in blends of d-PMMA and h-PMMA, where M_w(h-PMMA) $\approx$ 330 000 and M_w(d-PMMA) varies from 12 000 to 330 000. The degree of enrichment is very high (almost 100% d-PMMA at the surface), but the surface

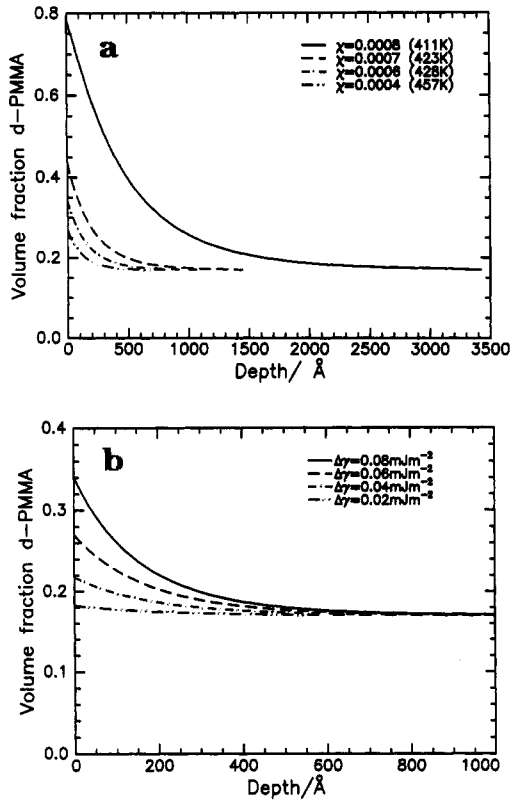

Figure 7. Theoretical composition profiles calculated from the expressions of Jones and Kramer for blend D. (a) Surface energy difference fixed at 0.08 mJ m^{-2} and χ varied over the range found for blend D (temperature in brackets is that at which the value of χ is found). (b) χ = 0.0006, the surface energy difference is varied from 0.08 mJ m^{-2} (the value found for the d-PS/h-PS blend).

excess is very small because the characteristic length of the enriched layer is very small (~10 Å). The authors make no mention of the background subtraction they have used, and the reflectivity profiles they show are characteristic of data from which no background has been subtracted. We suspect that the enrichment they observe is an artefact arising from incorrect background subtraction. In addition, the authors do not state the tacticity of their polymers, but the annealing temperature used was 120 °C, approximately 10 °C below the glass transition temperature of the polymers used by us but slightly above that of the polymers used by Liu *et al.*

Conclusions

We have studied the surface enrichment behavior of various low molecular weight probe d-PMMA in a high molecular weight matrix h-PMMA over a range of probe molecular weights and annealing times. Neutron reflectometry and SSIMS have been used to determine the surface and near-surface composition. We have observed no significant enrichment of either the h-PMMA or the d-PMMA at the air interface. This is attributed to an insufficient surface energy difference between the hydrogenous and deuterated polymers, in contrast to the behavior observed by other workers in the d-PS/h-PS system where deuteration does produce a large enough change in surface energy to drive considerable amounts of d-PS to the air surface.

Acknowledgment. R.W.R., I.H., S.A., M.H., and R.A.P. thank Courtaulds plc and the Science and Engineering Research Council for financial support, via a cooperative award, of the research program of which this work forms a part. We are grateful to Devinda S. Sivia for allowing us to use his maximum entropy profile fitting programs.

References and Notes

(1) Cahn, J. W. *J. Chem. Phys.* **1977**, *66* (8), 3667.
(2) Schmidt, I.; Binder, K. *J. Phys.* **1985**, *46*, 1631.
(3) Jones, R. A. L.; Kramer, E. J. *Polymer* **1993**, *34* (1), 115.
(4) Nakanishi, H.; Pincus, P. *J. Chem. Phys.* **1983**, *79* (2), 997.
(5) Carmesin, I.; Noolandi, J. *Macromolecules* **1989**, *22*, 1689.
(6) Wang, J. S.; Binder, K. *J. Chem. Phys.* **1991**, *94* (12), 8537.
(7) Cifra, P.; Bruder, F.; Brenn, R. *J. Chem. Phys.* **1993**, *99* (5), 4121.
(8) Hariharan, A.; Kumar, S. K.; Russell, T. P. *Macromolecules* **1991**, *24*, 4909.
(9) Hariharan, A.; Kumar, S. K.; Russell, T. P. *Macromolecules* **1990**, *23*, 3584.
(10) Kumar, S. K.; Russell, T. P. *Macromolecules* **1991**, *24*, 3816.
(11) Mills, P. J.; Green, P. F.; Palmstrom, C. J.; Mayer, J. W.; Kramer, E. J. *Appl. Phys. Lett.* **1989**, *54* (6), 590.
(12) Whitlow, S. J.; Wool, R. P. *Macromolecules* **1991**, *24*, 5926.
(13) Payne, R. S.; Clough, A. S.; Murphy, P.; Mills, P. J. *Nucl. Instrum. Methods Phys. Res., Sect. B* **1989**, *B42*, 130.
(14) Penfold, J.; Ward, R. C.; Williams, W. G. *J. Phys. E* **1987**, *20*, 1411.
(15) Bates, F. S.; Wignall, G. D. *Phys. Rev. Lett.* **1986**, *57* (12), 1429.
(16) Jones, R. A. L.; Norton, L. J.; Kramer, E. J.; Composto, R. J.; Stein, R. S.; Russell, T. P.; Mansour, A.; Karim, A.; Felcher, G. P.; Rafailovich, M. H.; Sokolov, J.; Zhao, X.; Schwarz, S. A. *Europhys. Lett.* **1990**, *12* (1), 41.
(17) Hariharan, A.; Kumar, S. K.; Russell, T. P. *J. Chem. Phys.* **1993**, *98* (5), 4163.
(18) Doi, M.; Edwards, S. F. *The Theory of Polymer Dynamics*; Clarendon Press: Oxford, U.K., 1986.
(19) de Gennes, P.-G. *Scaling Concepts in Polymer Physics*; Cornell University Press: Ithaca, NY, 1979.
(20) Lekner, J. *Theory of Reflection*; Martinus Nijhoff: Dordrecht, The Netherlands, 1987.
(21) Russell, T. P. *Mater. Sci. Rep.* **1990**, *5*, 171.
(22) Kunz, K.; Reiter, J.; Götzelmann, A.; Stamm, M. *Macromolecules* **1993**, *26*, 4316.
(23) Pedersen, J. S. *J. Appl. Cryst.* **1992**, *25*, 129.
(24) Peat, I. R.; Reynolds, W. F. *Tetrahedron Lett.* **1972**, *14*, 1359.
(25) Ferry, J. D. *Viscoelastic Properties of Polymers*, 3rd ed.; Wiley: New York, 1980.
(26) Sivia, D. S.; Hamilton, W. A.; Smith, G. S. *Physica B* **1991**, *173*, 121.
(27) Affrossman, S.; Hartshorne, M.; Jerome, R.; Munro, H.; Pethrick, R. A.; Petitjean, S.; Rei Villar, M. *Macromolecules* **1993**, *26*, 5400.
(28) Brinkhuis, R. H. G.; van Ooij, W. J. *Surf. Interface Anal.* **1988**, *11*, 214.
(29) Reiter, G.; Steiner, U. *J. Phys. II* **1991**, *1*, 659.
(30) Jinnai, H.; Hasegawa, H.; Hashimoto, T.; Han, C. C. *Macromolecules* **1992**, *25*, 2078.
(31) Bates, F. S.; Dierker, S. B.; Wignall, G. D. *Macromolecules* **1986**, *19*, 1938.
(32) Bates, F. S.; Wignall, G. D. *Macromolecules* **1986**, *19*, 934.
(33) Liu, Y.; Reiter, G.; Kunz, K.; Stamm, M. *Macromolecules* **1993**, *26*, 2134.
(34) Van Alsten, J. G.; Lustig, S. R. *Macromolecules* **1992**, *25*, 5069.
(35) Jones, R. A. L.; Kramer, E. J. *Philos. Mag. B* **1990**, *62* (2), 129.
(36) Hopkinson, I.; Kiff, F. T.; Richards, R. W.; King, S. M.; Munro, H. *Polymer* **1994**, *85*, 1722.
(37) Frantz, P.; Leohardt, D. C.; Granick, S. *Macromolecules* **1991**, *24*, 1868.
(38) Johnson, H. E.; Granick, S. *Macromolecules* **1990**, *23*, 3367.
(39) Van Krevelen, D. W. *Properties of Polymers*, 3rd ed.; Elsevier: New York, 1990.
(40) Tasaki, S.; Yamaoka, H.; Yoshida, F. *Physica B* **1992**, *180/181*, 480.

MA940997O